Proceedings of the ASME 2017 12th International Manufacturing Science and Engineering Conference
MSEC2017
June 4-8, 2017, Los Angeles, CA, USA

MSEC2017-2873

NUMERICAL MODELING OF GRAIN GROWTH IN LASER ENGINEERED NET SHAPING (LENS) OF AISI 316 STAINLESS STEEL

Wenda Tan and Xuxiao Li
Department of Mechanical Engineering
University of Utah
Salt Lake city, Utah, USA

ABSTRACT

A multi-scale modeling framework is developed in this work to simulate the transport phenomena and grain growth in Laser Engineered Net Shaping (LENS) process of austenitic stainless steel AISI 316. A three-dimensional (3D) model is included to simulate the transient molten pool geometry and heat/mass transfer on a macro-scale; and a 3D meso-scale model based on the Cellular Automata method is included to predict the grain growth during molten pool solidification. The predicted grain structure is found to be consistent with the experimental results and reveals that the grain structure is highly dependent on the molten pool geometry.

KEYWORDS

Laser engineered net shaping multi-scale modeling; heat/mass transfer; grain growth; Cellular Automata method.

1. INTRODUCTION

Laser Engineered Net Shaping (LENS) is a laser-based additive manufacturing process that has seen rapid development in the last one decade. This technique has been successfully employed to fabricate complex 3-dimensional (3D) components with a wide range of engineering materials, and has found numerous applications in defense, aerospace, automotive, and medical industries [1-3].

The microstructures in LENS products have been constantly of great interests to the academia and industry. Many LENS processing parameters, including laser power, laser scanning speed, patch distance, laser scanning pattern, among others, collaborate to determine the thermal history, which, in turn, have decisive effects on the microstructure in LENS products [4-6]. An experimental approach has been widely used to identify the processing-microstructure relationship in the LENS process. However, since the parameter space for the process is so large, experimental investigations usually demand high cost and long schedule. In order to reduce the expense, a numerical modeling approach has been increasingly used to identify the processing-microstructure relationship.

There have been extensive efforts to model the macro-scale thermal field evolution in LENS process. While some models were developed solely based on heat conduction equation [7-9], most models included fluid flow in the formulation for more comprehensive consideration of the underlying physics [10-15]. Additional algorithms have been used in most of these models to track the elevation of molten pool surface in LENS process: the element activation method has been used in finite-element models [7-9], while the volume-of-fluid method [10] and the level-set method [11-15] have been used in finite-volume models.

On the other hand, the modeling of microstructure evolution in LENS processes is still in its early stage. Both micro-scale Cellular Automata (CA) model and Phase Field (PF) model [15-18] have been used to simulate the dendrite growth in LENS process. The simulations results were quantitatively consistent with experiment results and have provided informative insight on the dendrite growth during the rapid solidification. However, due to the high computational cost of these models, most simulations have been limited to 2D domains and/or very limited sizes (~100 microns), which cannot reveal the 3D microstructure feature in LENS products of reasonable sizes.

In order to alleviate the computational demands, a meso-scale CA model has been used as a compromise. The meso-scale CA model was proposed to track the advancement of grain boundaries during solidification without considering the detailed dendrite growth within each grain [19]. This model was used to predict the grain growth during arc welding [20] and laser keyhole welding processes [21], and has recently been used in LENS and Selective Laser Melting (SLM) processes [22-24]. The modeling results well resembled the grain structure in the products of different processes. More importantly, this method is computationally efficient and can potentially be used to simulate the 3D grain growth in an entire LENS product.

In the present work, a multi-scale modeling framework is developed to investigate the LENS process. A macro-scale model is used to simulate the 3D transport phenomena in the molten pool and substrate. The temperature field is predicted by the macro-scale model and applied to a meso-scale model. The

meso-scale model is based on the Cellular Automata method to simulate the 3D grain growth during the solidification of the moving molten pool. This modeling framework is used to simulate a simple LENS process of AISI 316 stainless steel with only two tracks partially overlapped with each other, and the predicted grain structure is analyzed.

2. MODEL DESCRIPTION

2.1 Macro-scale Modeling of Transport Phenomena

In a LENS process as shown in Figure 1, a laser creates a molten pool that melts the substrate and the powder material fed thereon. The local molten material rapidly solidifies after the laser moves away, and forms a deposition layer bonding strongly with the substrate. The major physical phenomena in this process include laser absorption, molten pool surface deformation, and multi-phase heat/mass transport, all of which have been taken into account in a 3-dimensional (3D) macro-scale model [14, 15].

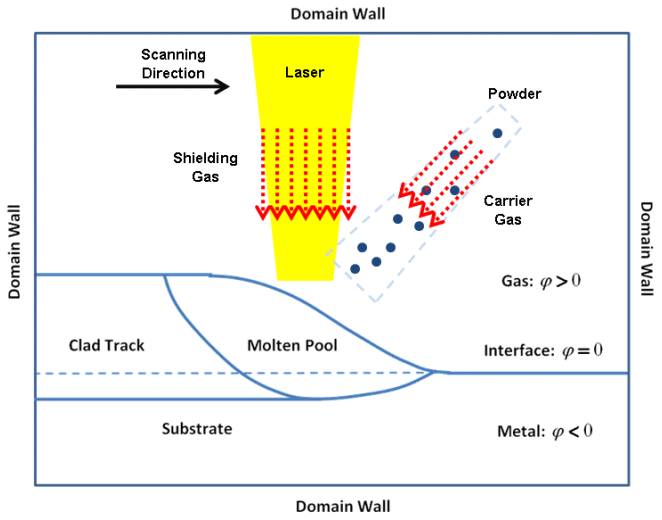

Figure 1: 2D schematic illustration of computational domain: the metal region, consisting of substrate, clad track and molten pool, has $\varphi < 0$, the gas region has $\varphi > 0$, and the metal/gas interface has $\varphi = 0$.

Molten Pool Surface Deformation

As shown in Figure 1, the molten pool, deposition layer, and substrate are classified into the metal region. The region above the metal, which is filled with shielding gas, carrier gas, and ambient air, is called the gas region. The deformation of the molten pool, which is the metal/gas interface, is tracked by a Level-Set (LS) equation (Eq. 1):

$$\frac{\partial \varphi}{\partial t} = -\left(\vec{V} + F_{\mathrm{P}} \cdot \vec{N}\right) \cdot \nabla \varphi \quad (1)$$

Here φ is the LS function. Any point on the interface of interest will have their LS values being zero, and the points off the interface will have their LS value being the signed distance between themselves to the interface. The sign is positive for the points in the non-condensed region, and negative for the points in the condensed region. On the right hand side (RHS) of the equation, $\vec{V}$ is the flow velocity of molten metal at the interface, F_{P} is the interface elevation speed caused by powder addition (predicted in [23]), and $\vec{N}$ is the normal direction of the interface.

Heat/Mass Transfer in Liquid and Solid Metal

The transport phenomena in the condensed metal region are calculated based on the conservation equations of mass, momentum, and energy (Equation 2 - Equation 4).

$$\frac{\partial}{\partial t}(\rho) + \nabla \cdot \left(\rho \vec{V}\right) = 0 \quad (2)$$

$$\frac{\partial}{\partial t}\left(\rho \vec{V}\right) + \nabla \cdot \left(\rho \vec{V} \vec{V}\right) = +\nabla \cdot \left(\mu \nabla \vec{V}\right) - \nabla p + S_M \quad (3)$$

$$\frac{\partial}{\partial t}(\rho h) + \nabla \cdot \left(\rho \vec{V} h\right) = \nabla \cdot (k \nabla T) + S_E \quad (4)$$

In the above equations, ρ is the mass density, $\vec{V}$ is the velocity, μ is the viscosity, p is the pressure, h is the material enthalpy, and k is the thermal conductivity. S_M is the source term for the momentum conservation equation, which can be formulated as Equation 5.

$$S_M = -\frac{\mu}{K}\vec{V} + \left(\nabla_s \sigma + \gamma \kappa \vec{N}\right)\delta_m(\varphi) \quad (5)$$

Here the first term on the RHS represents the damping effect when the fluid passes through the mushy region; the term $\nabla_s \sigma$ represents the thermos-capillary force; and the term $\gamma \kappa \vec{N}$ represents the capillary force. The thermo-capillary force and capillary force are applied with the help of a modified delta function [14, 15]. S_E is the source term for the energy conservation energy, which can be formulated as equation 6.

$$S_E = [Q_{laser} - \sigma \varepsilon (T^4 - T_\infty^4) - A_h (T - T_\infty)]\delta_m(\varphi) \quad (6)$$

Here Q_{laser} represents the distribution of absorbed laser power influx; $\sigma \varepsilon (T^4 - T_\infty^4)$ and $A_h (T - T_\infty)$ represent the radiative and convective heat loss on molten pool surface, respectively.

Note that the metal is assumed to be a continuum in the macro-scale model, with all the physical properties of the metal are calculated as weighted average of different phases according to the specific rules that have been introduced in [14, 15].

2.2 Meso-scale Modeling of Grain Growth

Once the 3D thermal history in the metal region is predicted by the macro-scale model, it is applied to a 3D meso-scale CA model [21] that simulates the competitive growth of multiple grains during the molten pool solidification.

In this model, the calculation domain is set to include the substrate as well as the fabricated part. The domain is meshed into a number of cubic cells with uniform size, and each cell carries the variables including temperature, cell state, and crystallographic orientation.

- The temperature is mapped from the thermal field predicted by the macro-scale model. Since the macro-scale model uses much larger mesh size than the meso-scale model does, linear interpolation is used to calculate the temperature value for each CA cell.
- The state of each cell can be solid, re-solid, liquid, solid/liquid (S/L) interface, and gas. At the beginning of the simulation, the cell state is initialized as either solid or gas, according to whether it is located inside or outside the substrate. These cells may change to liquid, interface and then to re-solid state according to specific rules, as will be

introduced later.

- The initial solid cells in the substrate belong to different grains, and each grain should contain multiple solid cells. All the solid cells in the same grain should have an identical crystallographic orientation (CO), which is the CO of this grain. For the AISI 316 stainless steel to be investigated in this work, the dominating phase in the substrate as well as in the weld zone is Austenite with the crystal lattice structure of face-centered-cubic (FCC). The FCC grains, if growing in a uniform temperature field, should maintain an envelope of a regular octahedron with equal growth preference along all the diagonal directions, as shown in Figure 2a. The CO of an FCC grain can be described by 3 Euler angles, Θ, Φ and Ψ, which quantify the angular relationship between the local Cartesian coordinate of a grain (X'-Y'-Z' in Figure 2b) and the global Cartesian coordinate of the computation domain (X-Y-Z in Figure 2b).

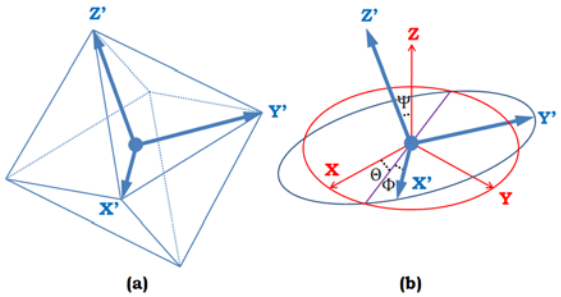

Figure 2: Grain shape and crystallographic orientation in 3D cellular automata model: (a) a grain grows with octahedron shape with equal preference along all diagonal directions; (b) the crystallographic orientation of a grain with respect to the global coordinate is defined by three Euler angles.

As a molten pool enters a certain region, some of the local solid cells will be heated to above the liquidus temperature. In this case the solid cells will be changed to liquid and their initial COs are erased, indicating the occurrence of melting. Due to the addition of metal powder, the top surface of the molten pool is elevated. The molten pool will catch some gas cells and turn them to liquid cells as well.

As the molten pool moves away, the local temperature will drop. If a liquid cell is located on the fusion line of the molten pool and its temperature falls below the liquidus temperature, this liquid cell will turn to an interface cells. Such interface cells, according to the epit-axial nucleation mechanism, will have their COs inherited from the closest solid neighbor cells that are not melted by the molten pool.

Starting from these "seed" interface cells, more and more liquid cells will turn to interface and then re-solid cells, replicating the solidification process. The process of liquid cells turning to interface cell is controlled by the de-centered square method [24]. As shown in Figure 3a, in a "seed" interface cell (cell boundary not shown), there is a growing octahedron envelope centered at point A. One diagonal of this envelope is aligned along the CO of this cell with respect to the global coordinate. The length of all the half-diagonals of this envelope, denoted by L in Figure 3a, can be calculated by integrating the grain growth velocity over time, as shown in Equation 7.

$$L = \sum[V_g \cdot \Delta t] \quad (7)$$

Here V_g is the grain growth velocity; Δt is the time step of the CA model. At the end of a specific time step, the envelope will become large enough so that one corner of the envelope will reach point B in the neighboring cell (cell boundary not shown), as shown in Figure 3b. If this neighboring cell is liquid, it will be captured by the "parent cell" as a new interface cell. A new envelope centered at point B will start growing in the new interface cell, as denoted by the red octahedron in Figure 3c. This envelope will grow with its own velocity as a function of its own temperature, and capture other liquid cells in its neighborhood to become new interface cells. When an interface cell is totally surrounded by other interface cells, this interface cell will change its state to re-solid.

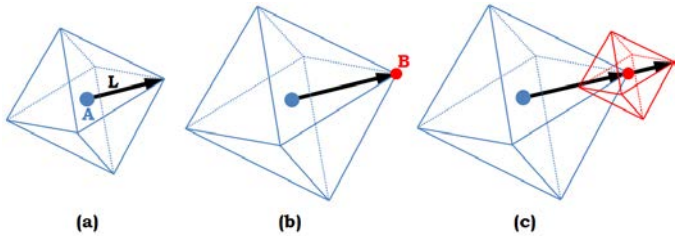

Figure 3: Schematic illustration of 3D De-center square algorithm: (a) parent cell expand its octahedron envelope; (b) parent envelope capture new interface cell; (c) new interface cell expands its own octahedron envelope.

Following the above algorithm, some "seed" interface cells will be generated at the fusion line of the molten pool, with their COs inherited from the un-melted solid neighboring cells. Starting from these "seed" cells, a chain process will be triggered to get all the liquid cells turning to interface and then re-solid cells. Each re-solid cells will have a specific CO inherited from one of its neighbor cells. The re-solid cells with the same orientation reconstruct the shape of a grain, thus the shapes of all the grains in the re-solidified weld zone can be simulated.

The grain growth velocity in Equation 7, V_g, is assumed to be correlated with solely temperature, as shown in Equation 8.

$$V_g(\Delta T) = 7.325 \times 10^{-6} \times \Delta T^{3.12} \quad (8)$$

Here ΔT is the undercooling of each interface cell, i.e. the difference between its actual temperature and the liquidus temperature of the metal. The correlation is obtained from the numerical modeling results from a Cellular Automata-Phase Field model, which was developed to simulate the dendrite growth of multi-component alloys [21].

3. RESULTS AND DISCUSSION

This multi-scale modeling framework is applied to a simple LENS case of two tracks partially overlapped with each other with a hatch distance of 350 μm. The laser power is 300 W, the laser spot size is 500 μm, the laser scanning speed is 12.7 mm/s, and the powder feed rate is 7 g/min. Both the substrate and powder are AISI 316 stainless steel, with the physical properties given in [14, 15]. One snapshot of the predicted thermal field by

the macro-scale model is shown in Figure 4. The 3D thermal history is then applied to the meso-scale CA model for the prediction of 3D grain growth in the two tracks.

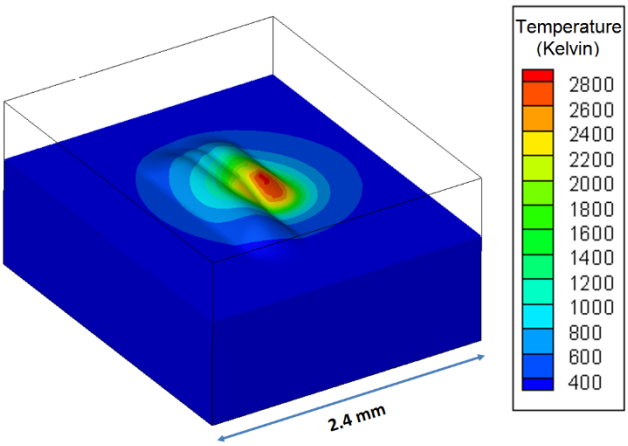

Figure 4: Snapshot of thermal field prediction by macro-scale model.

Shown in Figure 5 are the longitudinal sections of the predicted grain structure in the two tracks along their center planes. The two sections show very similar grain patterns: the grains grow almost vertically upward in the lower portion of the fusion zone, and turn horizontal in the upper portion of the fusion zone. This pattern is also qualitatively consistent with the experimental and numerical results in Figure 6, which was presented in [15]. Competitive grain growth exists in the solidification of fusion welding as well as LENS and SLM. The directional solidification in these processes will favor the grains whose COs align better with the local temperature gradient. These favored grains tend to grow faster and crowd out other less favored grain. As the molten pool is moving forward, the grains start epit-axial growth from the bottom of the molten pool, where the temperature gradient is mostly upward. The favored grains will be those with their COs pointing upward, and they grow upward and block the growth of other grains. As the molten pool moves forwards and the molten pool tail arrives, the grains from the bottom of the molten pool have all grown to a certain height (marked out by the dashed line in Figure 5). After this moment the temperature gradient becomes almost parallel to the laser scanning direction, and hence the grains are forced to grow horizontally, even though this direction may not be well aligned with their COs.

Shown in Figure 7 are the predicted grain structure on one cross-section of the two tracks. In the first track, the lower portion of the fusion zone is dominated by columnar grains aligned along the vertical direction, which are generated by the epit-axial growth. On the upper part, many “equi-axed” grains can be found, which are actually the cross-sections of those columnar grains that grow horizontally (as have been found in the upper portion of the longitudinal section in Figure 5).

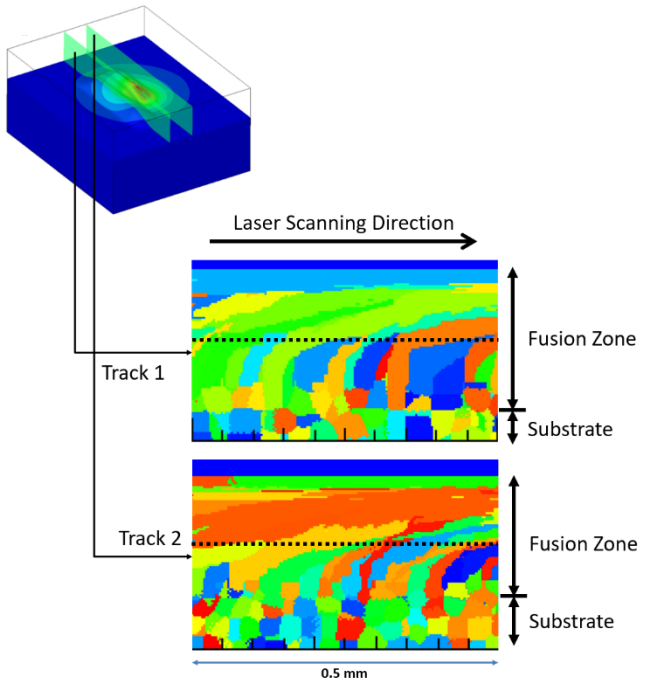

Figure 5: Grain structure predicted on the longitudinal section on the center planes of the two tracks.

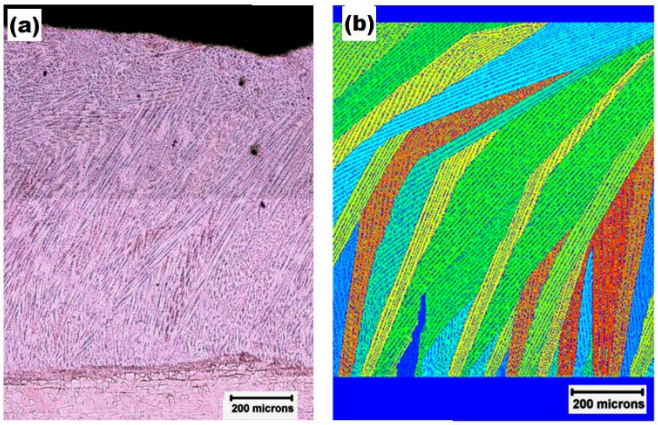

Figure 6: Microstructure in longitudinal section in LENS process: (a) experiment result and (b) numerical modeling of dendrite morphology [15].

In the second track, a similar grain pattern can be found on the right half of the track: columnar grains start their epit-axial growth from the fusion line and develop vertically, and was blocked by other columnar grains that grow horizontally in the upper portion of the fusion zone. In the meantime, a different grain pattern can be found on the left portion of the second track, where the second track overlaps with the first track. In this overlap region the second track will re-melt a portion of the first track, and the epit-axial nucleation will start from the grains in the first track. Note that the grains in the first track are different from those in the substrate: they are mostly columnar grains with their COs already selected during the solidification of the first track; while the grains in the substrate are usually equi-axed with random COs. It is also interesting to find that the grains in this

region develop horizontally. Due to the pre-existence of the first track, the fusion line of the second track (also marked out by the dashed line in Figure 7) is not as "horizontal" as in the first track. The local temperature gradient has a significant horizontal component, which drives the local grains to develop horizontally instead of vertically.

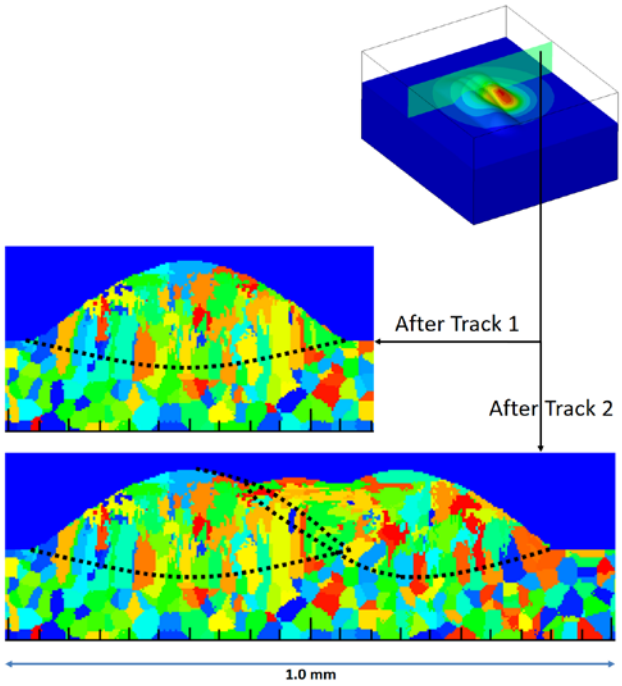

Figure 7: Grain structures predicted by meso-scale model on cross-section of the two tracks.

Through the investigation of this simple case with only two tracks, it is demonstrated that the grain growth in LENS is a highly 3D process, which is difficult to be captured by 2D models. The multi-scale modeling framework presented here is capable of predicting the process. This work is expected to be expanded to simulate the 3D grain growth in LENS process with multi-tracks and multi-layers.

4. CONCLUSION

In the present paper, a multi-scale modeling framework has been developed to simulate the 3D heat/mass transport and grain growth in Laser Engineered Net Shaping (LENS) process of AISI 316 stainless steel. The macro-scale evolution of temperature and velocity field during the LENS process was captured by a transient numerical model that combines level-set equation and the thermos-hydrodynamic equation set. The meso-scale grain growth was simulated with the Cellular Automata method. The thermal field predicted by the macro-scale model was applied to the meso-scale CA model, and reasonable grain structure was predicted by the model. It was demonstrated that the grain growth in LENS process is a highly 3D process. The competitive grain growth dominates the grain selection during solidification. The grain orientation is highly dependent on the molten pool shape and varies throughout the molten pool.

5. ACKNOWLEDGMENTS

The authors wish to gratefully acknowledge the financial support provided for this study by the startup funds from the University of Utah and the technical support from the Center for High Performance Computing at the University of Utah.

REFERENCES

[1] Gibson, I., Rosen, D.W. and Stucker, B., 2010. *Additive manufacturing technologies*. New York: Springer.
[2] Frazier, W.E., 2014. Metal additive manufacturing: a review. *Journal of Materials Engineering and Performance*, *23*, pp.1917-1928.
[3] Gao, W., Zhang, Y., Ramanujan, D., Ramani, K., Chen, Y., Williams, C.B., Wang, C.C., Shin, Y.C., Zhang, S. and Zavattieri, P.D., 2015. The status, challenges, and future of additive manufacturing in engineering. *Computer-Aided Design*, *69*, pp.65-89.
[4] Parimi, L.L., Ravi, G.A., Clark, D. and Attallah, M.M., 2014. Microstructural and texture development in direct laser fabricated IN718. *Materials Characterization*, *89*, pp.102-111.
[5] Yadollahi, A., Shamsaei, N., Thompson, S.M. and Seely, D.W., 2015. Effects of process time interval and heat treatment on the mechanical and microstructural properties of direct laser deposited 316L stainless steel. *Materials Science and Engineering: A*, *644*, pp.171-183.
[6] Wang, Z., Palmer, T.A. and Beese, A.M., 2016. Effect of processing parameters on microstructure and tensile properties of austenitic stainless steel 304L made by directed energy deposition additive manufacturing. *Acta Materialia*, *110*, pp.226-235.
[7] Costa, L., Vilar, R., Reti, T. and Deus, A.M., 2005. Rapid tooling by laser powder deposition: Process simulation using finite element analysis. *Acta Materialia*, *53*, pp.3987-3999.
[8] Wang, L. and Felicelli, S., 2007. Process modeling in laser deposition of multilayer SS410 steel. *Journal of Manufacturing Science and Engineering*, *129*, pp.1028-1034.
[9] Peyre, P., Aubry, P., Fabbro, R., Neveu, R. and Longuet, A., 2008. Analytical and numerical modelling of the direct metal deposition laser process. *Journal of Physics D: Applied Physics*, *41*, p.025403.
[10] Choi, J., Han, L. and Hua, Y., 2005. Modeling and experiments of laser cladding with droplet injection. *Journal of Heat Transfer*, *127*, pp.978-986.
[11] Han, L., Phatak, K.M. and Liou, F.W., 2004. Modeling of laser cladding with powder injection. *Metallurgical and Materials Transactions B*, *35*, pp.1139-1150.
[12] Zhang, H.O., Kong, F.R., Wang, G.L. and Zeng, L.F., 2006. Numerical simulation of multiphase transient field during plasma deposition manufacturing. *Journal of applied physics*, *100*, p.123522.
[13] Qi, H., Mazumder, J. and Ki, H., 2006. Numerical simulation of heat transfer and fluid flow in coaxial laser cladding process for direct metal deposition. *Journal of applied physics*, *100*, p.024903.
[14] Wen, S. and Shin, Y.C., 2010. Modeling of transport phenomena during the coaxial laser direct deposition process.

Journal of Applied Physics, *108*, p.044908.
[15] Tan, W., Wen, S., Bailey, N. and Shin, Y.C., 2011. Multiscale Modeling of Transport Phenomena and Dendritic Growth in Laser Cladding Processes. *Metallurgical and Materials Transactions B*, *42*, pp.1306-1318.
[16] Yin, H. and Felicelli, S.D., 2010. Dendrite growth simulation during solidification in the LENS process. *Acta Materialia*, *58*, pp.1455-1465.
[17] Fallah, V., Amoorezaei, M., Provatas, N., Corbin, S.F. and Khajepour, A., 2012. Phase-field simulation of solidification morphology in laser powder deposition of Ti–Nb alloys. *Acta Materialia*, *60*, pp.1633-1646.
[18] Nie, P., Ojo, O.A. and Li, Z., 2014. Numerical modeling of microstructure evolution during laser additive manufacturing of a nickel-based superalloy. *Acta Materialia*, *77*, pp.85-95.
[19] Gandin, C.A. and Rappaz, M., 1994. A coupled finite element-cellular automaton model for the prediction of dendritic grain structures in solidification processes. *Acta Metallurgica et Materialia*, *42*, pp.2233-2246.
[20] Chen, S., Guillemot, G. and Gandin, C.A., 2016. Three-dimensional cellular automaton-finite element modeling of solidification grain structures for arc-welding processes. *Acta Materialia*, *115*, pp.448-467.
[21] Tan, W. and Shin, Y.C., 2015. Multi-scale modeling of solidification and microstructure development in laser keyhole welding process for austenitic stainless steel. *Computational Materials Science*, *98*, pp.446-458.
[22] Zhang, J., Liou, F., Seufzer, W. and Taminger, K., 2016. A coupled finite element cellular automaton model to predict thermal history and grain morphology of Ti-6Al-4V during direct metal deposition (DMD). *Additive Manufacturing*, *11*, pp.32-39.
[23] Wen, S.Y., Shin, Y.C., Murthy, J.Y. and Sojka, P.E., 2009. Modeling of coaxial powder flow for the laser direct deposition process. *International Journal of Heat and Mass Transfer*, *52*, pp.5867-5877.
[24] Wang, W., Lee, P.D. and Mclean, M., 2003. A model of solidification microstructures in nickel-based superalloys: predicting primary dendrite spacing selection. *Acta materialia*, *51*, pp.2971-2987.